Chapter 3
Rotorcraft Propulsion Systems

Antonio Filippone and Nicholas Bojdo

Abstract This chapter introduces rotorcraft engines. the discussion is largely limited to gas turbine engines that dominate the field of modern helicopters. The Chapter is split into four main parts: (1) rotorcraft power plants and power trains; (2) engine ratings (with certification requirements); (3) performance envelopes; (4) intake protection systems. Rotorcraft engines are seldom treated as part of core rotorcraft engineering, since they are considered an element of propulsion; thus, they are associated to a different discipline. In this Chapter we demonstrate that there are peculiarities in this type of engines. Their integration into the airframe via transmission systems, rotor head, intake separators is unlike any fixed-wing vehicle.

Nomenculture

EGT	Exhaust gas temperature
IBF	Inlet barrier filter
IPS	Inertial particle separator
LTO	Landing and take-off
MCP	Maximum continuous power
MEP	Maximum emergency power
MTOP	Maximum take-off power
nvPM	Non-volatile particulate matter
OAT	Outside air temperature
TAS	True air speed (called V in equations)
SFC	Specific fuel consumption
UHC	Uncombusted hydrocarbons
VTS	Vortex tubes separator

A. Filippone (✉) · N. Bojdo
School of Engineering, The University of Manchester, Manchester, UK
e-mail: a.filippone@manchester.ac.uk

EI	Emission index
A_e, B_e	Coefficients in Eq. 3.3
c_1, c_2	Empirical factors in pressure loss Eq. 3.7
$C_{1,c}$	Dust concentration
d_p	Particle diameter
k_{loss}	Power loss in a gearbox
k_1, k_2	Lower loss factors
M	True Mach number
n	Number of operating engines
N_b	Number of blades or vanes per stage
N_{gg}	Gas generator turbine speed, rpm
N_p	Power turbine speed, rpm
P	Engine power, kW
P_s	Engine power, SHP
$\mathscr{R}$	Gearbox reduction ratio
t	Time, s
T, T_1	Air temperatures, K
T_3	Total gas temperature at compressor exit, K
T_4	Total gas temperature at combustor, K
W	Gross or take-off weight, kg
W_1	Air flow rate, m^3/s
W_{f6}	Fuel flow per engine, kg/s
z	Flight altitude (m or feet)

Greek Symbols

δ	Relative air pressure
η_s	Particle separation efficiency
θ	Relative air temperature
Π	Overall pressure ratio
σ	Relative air density
τ	Time constant of engine deterioration
ω	Total pressure loss coefficient
$\overline{(.)}$	Mean value
$(.)_i$	Index counter
$(.)_{AP}$	Engine in final approach
$(.)_{ID}$	Engine in idle
$(.)_{TO}$	Engine in take-off
$(.)_{sl}$	Sea level

3.1 Rotorcraft Power Plants

The great majority of helicopter power plants is made of gas turbine engines tuned for delivery of torque. These engines are called *turboshaft*. They have become popular in the 1960s, with rapid advances in gas turbine engine technology. Prior to that time, helicopters were powered by Internal Combustion (IC) engines. IC engines are nowadays limited to historic aircraft (for example, the *Sikorsky S-55* and the *Kamov Ka-26*) and to light modern aircraft (for example, the *Robinson R-22* and the *Schweitzer S300*). In recent years there has been research to reinvigorate the use of IC engines on rotorcraft, with initiatives that addressed the development of diesel engines. The outlook for the future is possibly different, with new types of rotorcraft being proposed, some sub-scale, both manned and unmanned, that are to be powered by electrical machines or by hybrid systems. Electrical tail rotors have been proposed. The technology is in rapid development, but for the time being gas turbine engines are the only realistic options for full scale, heavy lift and military rotorcraft.

The first gas turbine helicopters were the French Sud Aérospatiale *Alouette II* in 1956–1957, powered by a Turbomeca *Artouste*, and the Bell UH-1A *Iroquois* powered by a Lycoming T53-L-1 engine, around the same time (the exact dates are a matter of dispute). The now historical Sikorsky S-55 is a particularly interesting example of IC engine integration into a rotorcraft. Figure 3.1b shows a photo of one such vehicle. The engine exhaust is a large pipe at the front of the airframe pointing right (from the pilot's view). The engine itself was mounted at the front of the aircraft, and the main shaft runs through the cabin to engage the main gearbox on top of the fuselage, Fig. 3.1b. Getting into one pilot's seat may require ducking under the main shaft to climb out onto the other side.

One of the key limiters of the IC engines is the relatively low power/weight, higher specific fuel consumption and large dimensions. Modern turboshaft engines offer very high power/ratio performance are extremely compact and can be coupled in twin- and three-engine configurations. An example of turboshaft cut-out diagram is shown in Fig. 3.2.

Rotorcraft engine configurations are very compact. The lack of space available on the aircraft has forced engineers to find ever more ingenious solutions to integrate the engine onto the airframe and the rotor system. Twin-engine configurations are normally mounted side-by-side. Three-engine configurations generally have two engines mounted side-by-side and one central engine, often mounted higher and aft (most Mil helicopters, the CH-53, the AW101, and their variants). The intakes are generally front-facing, though not always, and the exhausts are forced either backwards or sideways. Upwards exhausts would interfere with the rotor and would damage the blades [1]; downwards exhausts are an operational hazard and would prevent many operations requiring engines running.

Important elements in the engine-airframe integration include the full transmission system, the fuel systems and the engine cooling system (lubrication pumps, oil and afferent lines). We will describe briefly some of these systems.
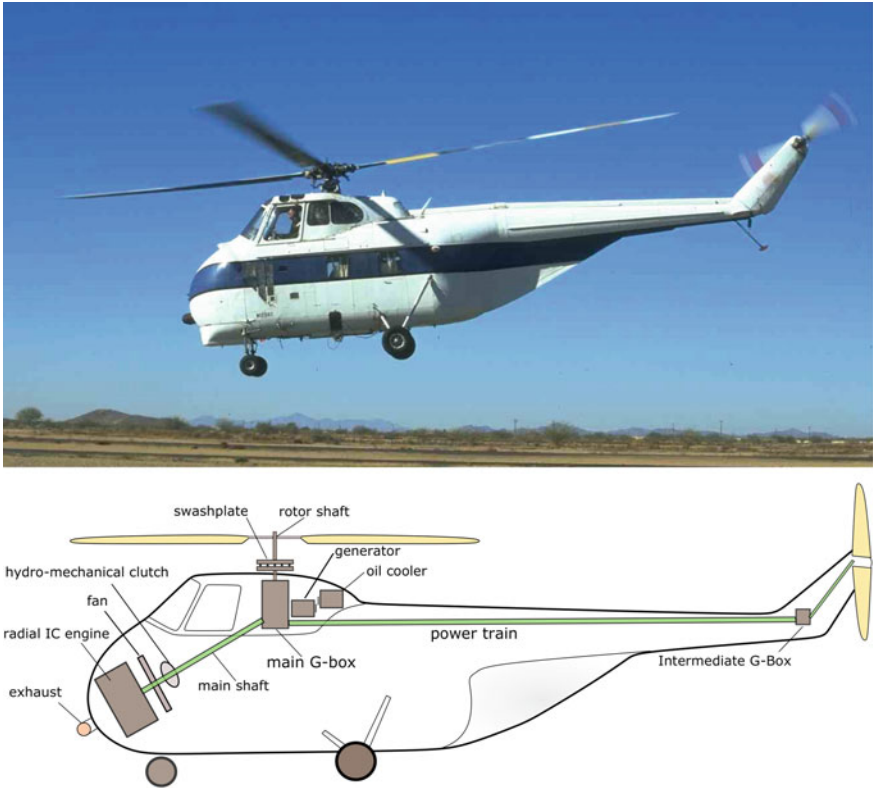
Fig. 3.1 Author's photo (circa 1997) and diagram of the Sikorsky S-55 transmission system. Main shaft running through the cabin
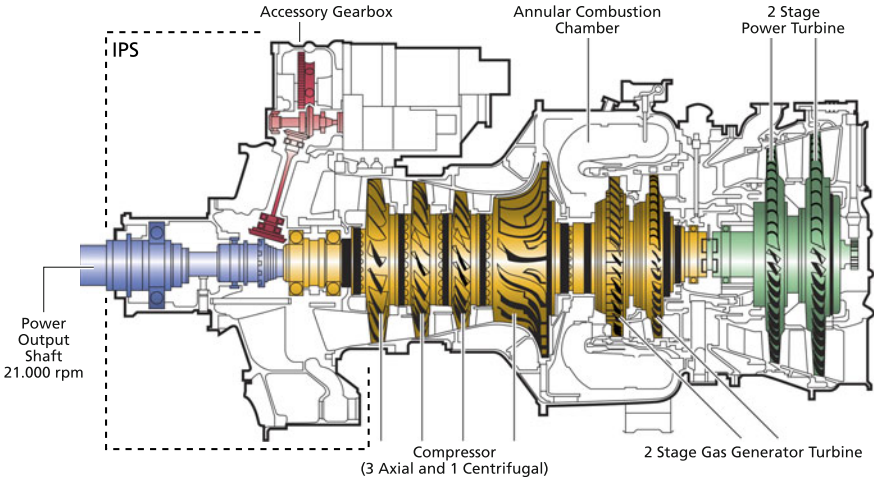

Fig. 3.2 Diagram of the the RTM322 turboshaft engine, adapted from a marketing brochure

Modern helicopter engines have a full electronic control system called FADEC, which is a hardware-software kit that allows full control and health monitoring of the engine. Several sensors in critical sections of the engine include temperature gages, pressure gages, and accelerometers. Add-ons include the intake protection systems, which are discussed in Sect. 3.5.

3.1.1 Architecture of a Turboshaft Engine

Torque-delivering gas turbine engines are classified as turboprops and turboshafts. The main difference between the two configurations is that the turboprop is suited to fixed-wing aircraft and delivers some residual thrust through the exhausts. This residual thrust makes up a non-negligible fraction of the net thrust, up to 10% or more at full throttle on the ground. The turboshaft is designed specifically for rotorcraft applications and does not provide any meaningful thrust in the exhaust. The key aspect of this engine is the ability to deliver as much torque as possible, which is then transferred to the rotor system.

Turboshaft engines have typically two main shafts. A gas-generator shaft consists of a gas turbine with a multi-stage compressor. The gas turbine can be a single- or multiple stages, depending on the engine rating. The multi-stage compressor has a number of axial compressor stages followed by a single-stage centrifugal compressor (or impeller). The reason why there is such a complicated turbomachinery is that centrifugal compressors deliver high compression ratios in a single stage and therefore are compact, whilst boosting the gas pressure to sufficient levels before it enters the combustion chamber. This group of turbomachinery rotates at very high rpm, and the design speed is called N_{gg} ('gg' is for gas generator). This rpm is often given in percent of the design rpm.

For reasons unknown to this author, overall compression ratios of turboshaft engines are seldom advertised, unlike turbofan engines. In any case, a modern single-stage axial compressor would have a compression ratio ~ 1.3, and a centrifugal impeller would have a compression ratio ~ 6.5. Therefore, the engine shown in Fig. 3.2 would be expected to have an overall compression ratio of $\Pi = 14.2$–14.5, unless otherwise specified by the manufacturer.

A co-axial shaft couples another gas axial turbine (single or multi-stage) with the output shaft, which then delivers power to the main rotor via a series of gear boxes. The angular speed of this shaft is virtually constant, but there are margins of short-term variation, for example within the range 95–110%. This angular speed is called N_p ('p' is for power turbine). If the torque on the output shaft increases, so it does too on the coupled gas turbine. The increase in torque would tend to slow down the turbine, that that can be prevented by increasing the fuel flow, which increases the mass flow rate of the hot gases through the turbine until the torque is restored. *Helicopter rotor speeds are constant, regardless of power output, with the exception of sharp increase/decrease in torque.*

An estimate of the power losses in the gear-box is done with the following assumptions. If the reduction-ratio is $\mathcal{R} = Q_{out}/Q_{in}$, and Q denotes the torque

$$k_{loss} = \frac{P_{in}}{P_{out}} = \frac{1}{\mathcal{R}} \left(\frac{Q_{in}}{Q_{out}} \right) = f(Q_{in}) \simeq k_1 \left(\frac{Q_{in}}{Q_{design}} \right)^2 + k_2 \qquad (3.1)$$

where k_{loss}, k_1 and k_2 are loss factors. Equation 3.1 implies that there is a floor in the power losses and that these losses increase with the input torque, which is normalised with the design torque. The term k_2 takes into account the fact that for small values of the torque, no output is expected, due to internal losses in the gear-box; the factor k_1 is to be determined experimentally, as it depends on the specific gear-box geometry.

3.2 Transmission and Power Train

The power transmission diagram of a modern helicopter is shown in Fig. 3.3. There is a gear-box to reduce the high speed of the engine shaft to a relatively low speed of the main rotor (reduction of 1:20 is not unusual). There is also a direct coupling of the main and tail rotor, via the gear-box and a central shaft, so that the two rotors rpm are locked.

The twin-engine configuration has a peculiar design. The availability of two engines would by itself not be a major engineering breakthrough if it were not for the direct coupling of two engine shafts to a main power train. One example of this architecture is shown in Fig. 3.3 for the AS-332 *Super Puma*, a helicopter that often operates in challenging environments over open ocean. There is a left and right engine, with shaft outputs at very high speed, $N_p = 22{,}841$ rpm. These shafts engage a main central/horizontal shaft through a series of gears and free-wheels that reduce the rpm to 4,888 rpm (reduction ratio approximately 1:4.5). There is a main gear box just ahead of the central shaft that through a series of epicyclical gears delivers torque at 265 rpm (rotor design speed). The tail rotor is coupled with the central shaft through a series of gear boxes: an intermediate gear box changes the direction of the transmission and the final tail rotor gear box delivers power at 1279 rpm. The ratio between tail- and main rotor speeds is a fixed ratio of 4.826.

Should one engine shut down because of damage, fire or other reasons, the remaining engine still engages the central shaft and delivers torque to the main- and tail rotor. The inoperative engine must be disengaged, in order to remove any residual torque that has to be overcome by the remaining engine. The system is called *spragg clutch*. Other elements are indicated an the graph, but are not described further (rotor brake and auxiliary systems). The important point to take from this discussion is that the helicopter can continue to operate with a single engine, assuming that it can deliver the required torque until an emergency landing is performed.

An interesting case is the power train of the *Boeing-Vertol CH-47*, as displayed in Fig. 3.4. As the case previously discussed of the twin-engine conventional helicopter, there is a redundancy system to prevent a total collapse in case of one engine failure.
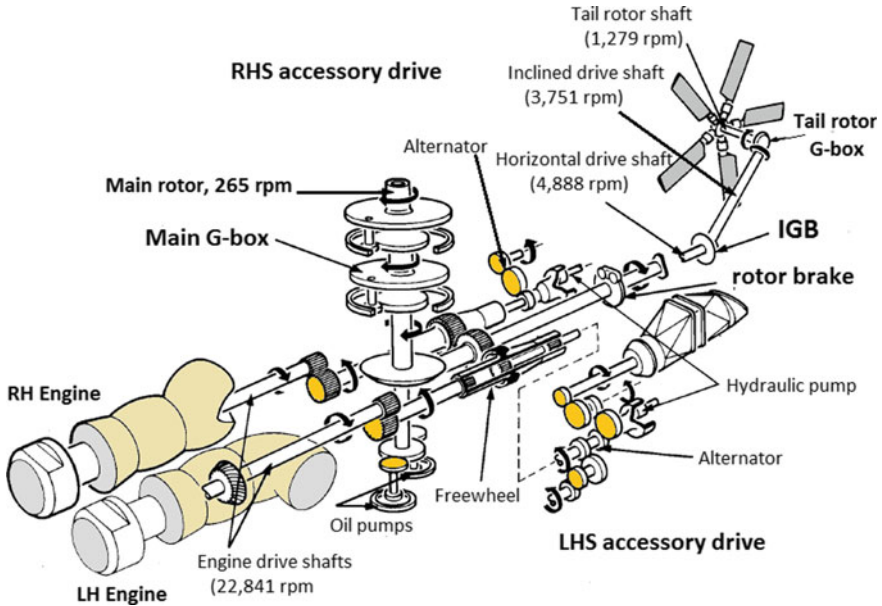
Fig. 3.3 Diagram of the transmission system of the Eurocopter/Airbus AS-332. Adapted from the Flight Crew Operating Manual
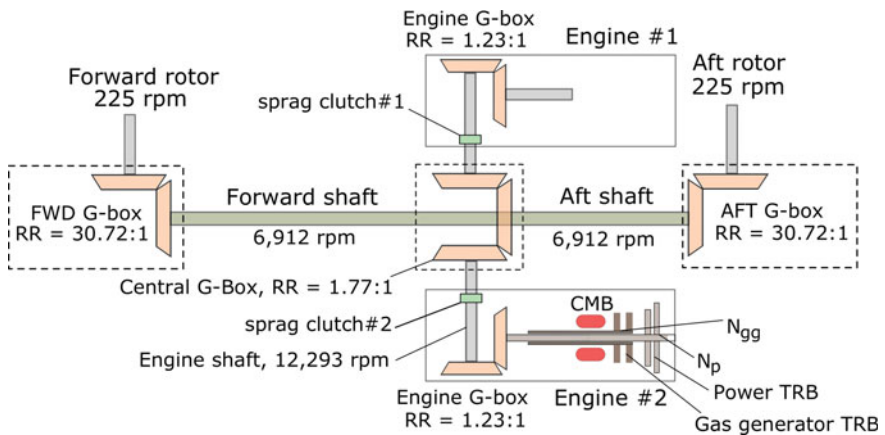

Fig. 3.4 CH47 helicopter drive train architecture; RR = reduction ratio

The architecture is based on the concept that two engines engage a central shaft, which then delivers torque to separate shafts. There is a spragg clutch per engine to allow disengagement, and a series of gear-boxes that reduce the engine shaft rpm to the much lower rotor 225 rpm. The total speed reduction is 1:54.64.

Among the twin rotor systems, notable is the power train of tilt-rotor aircraft, one embodiment of which is discussed by Wilson [2]. A tilt-rotor such as the Boeing V-22 is unlikely to be able to hover on a single engine. However, the central shaft system distributing torque through engine gear-boxes and a central gear-box dampens large torque imbalances and improves lateral stability.

Electrical tail rotors, and even multiple tail rotors have been proposed to take advantage of the efficiency of electrical machines. This new technology requires considerable changes in the transmission architecture, for example the inclusion of an electrical generator, power converters, electric cabling and control software. In principle, there are advantages in these new systems, such as the ability to disengage the tail rotor whilst idle on the ground (to save fuel and reduce noise), and the ability to operate at variable rpm, and thus optimise performance and reduce fuel consumption in level flight.

3.2.1 Gearbox Considerations

Gearboxes are critical and very heavy components, but there is no way of eliminating their presence, considering the very high speeds of the turboshaft engines. They are designed to deliver a maximum torque, and have a certified transmission limit, Q_{lim}. In any case, *the gear-box limit torque must exceed, by a reasonable amount, the maximum torque that can be delivered by the turboshaft engines*, Q_{shaft}.

If at some point the turboshaft are re-engineered to deliver a higher torque, it would be an advantage to have a gear-box that can sustain the upgrade. There is a limit to which this can happen, because it would imply that gear-boxes may have to be over-designed for their intended application. For example, the AW101 has a torque limit[1] of 112% of its design value for a a maximum continuous power output; this value increases to 118% for 2.5-min output rating.

Clearly, all of the power goes through the gear-box, and this creates problems in lubrication, heating and cooling. In fact, all losses in the gear-box are turned into heat. For example, with a 2000 kW of output power, a small 1% loss corresponds to 20 kW of heat that must go somewhere. Since the energy E is the power dissipation per unit time, $E = P \cdot t = 1.2$ MJ. With ~ 10 kg of aero engines lubricant, we would have a temperature increase of ~ 2–3 K/min. Hence, cooling is a requirement on all gear-boxes.

Some data exist in the technical literature on helicopter transmission weights [3], but this research is rather old (early 1980s), and is in need of an update. With the few data that are available in the open domain, it appears that the transmission weight grows linearly with the installed shaft power, Fig. 3.5.

---

[1] FAA Type Certificate Data Sheet H80EU, Revision 1, Feb. 2007.
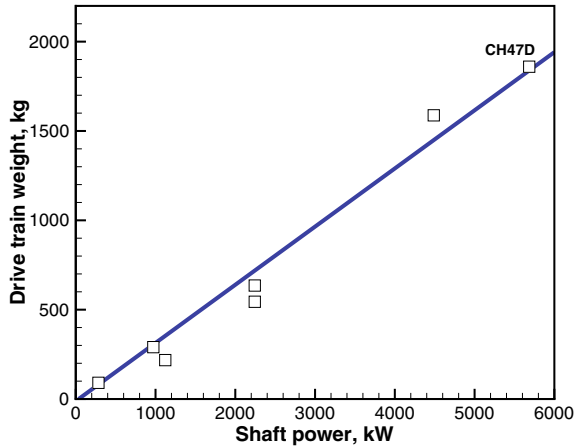
Fig. 3.5 Helicopter drive train weights (estimated)

3.3   Engine Power Ratings and Limitations

Turboshaft engines are certified by national and international bodies (FAA, CAA, EASA, US military, etc.) as other aero engines. They are characterised by different power ratings, that is necessary to specify. These power ratings will appear on the *Type Certificate*. Single-engine helicopters have turboshafts rated to power $< 1000\,\text{kW}$.

The data included in this document are engine architecture, power ratings, engine speeds, engine limitations (including temperatures in sections of the engine), fuels and lubricants allowed, key dimensions, weight and reference to technical documentation. There are notable differences in engine type certificates between the FAA and the EASA, and between revisions, and it is always interesting to compare both in order to extract as much information as possible.

To begin with, engine manufacturers do not know what the installation issues are. The same engine can be installed on different helicopters with different intake configurations. There is some exchange of data between engine manufacturers and airframe manufactures, but there are restrictions. Thus, we have the *uninstalled* engine power. This is to be measured in reference conditions: sea level, standard day. Furthermore, some *Type Certificates* establish the specific conditions of the output ratings, which may include the fuel heat capacity, bleed extraction (if any), accessory loads, inlet pressure recovery, and exhaust discharge conditions. The key power ratings are:

- Maximum continuous power (MCP): this is the power that can be delivered indefinitely, e.g. for any length of flight, without measurable performance deterioration.
- Maximum take-off power (MTOP): this is a power output that can be delivered for 5 minutes, which is a general estimate for the duration of take-off and initial stages of climb-out.
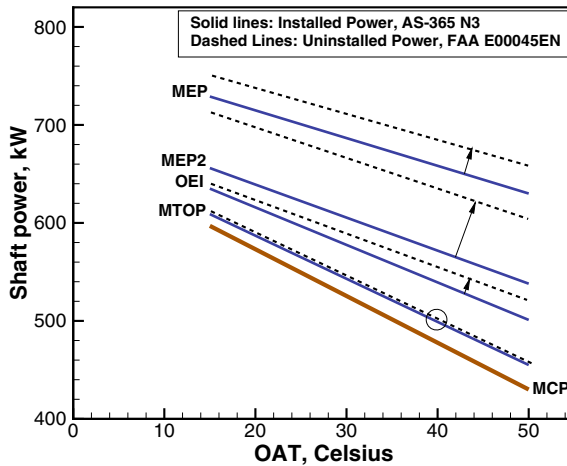
Fig. 3.6 Performance charts of the Turbomeca Arriel 2C2 turboshaft engine

- Emergency power rating (MEP): for a limited time (30 s, 2 min or otherwise), turboshaft engines can operate at increasing output to meet emergency situations. These events cause excessive heat, pressure and mechanical loads, and may need to be inspected before going back to service. This rating is sometimes called OEI rating.

In Fig. 3.6 we show the effects of engine power ratings, Outside Air Temperature (OAT), and installation effects, some of which will be discussed further. The documentation used for the preparation of this chart is indicated in the caption. For a fixed air temperature, note that the MCP is hardly affected by installation losses. These losses become materially important as we refer to shorter time frames and higher output ratings.

Another important effect is that of the air temperature. This engine (like any turboshaft) suffers from an increase in temperature (reduction in ambient air density), and on a hot day it can only deliver a fraction of its power on a standard day. Hence, hot day operations can be severely limited. Net out power depends on several factors, which include gas turbine discharge temperature (either TT4.5 or TT5), engine speed limits (N1%) and fuel flow limits (Wf6). This is illustrated in Fig. 3.7. The intermediate engine speed limit is quite narrow and now always clearly identifiable in engine test data. This behaviour is not shown in the data in Fig. 3.6, which are limited to higher OAT.

One engine can have military and civilian applications. For example, the Rolls-Royce/Allison M250 corresponds to the military engine T63. Furthermore, turboshaft can be developed into turboprops. For example, the General Electric T700 evolved into the CT7 turboprop (SAAB 340B), but there is a large series of engines within this family of turboshafts and turboprops.[2] Turboshaft engines evolve over a long time,

---

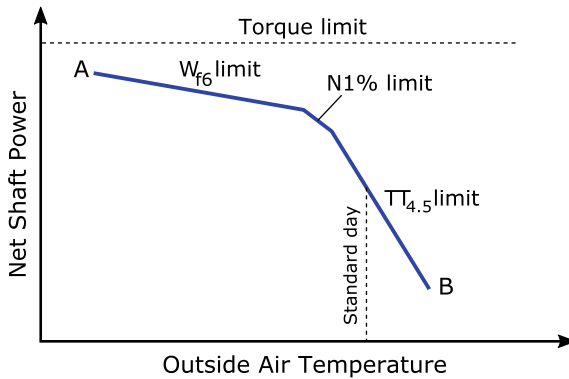[2] EASA Type Certificate Data Sheet E.010.

Fig. 3.7 Turboshaft engine power limits as function of outside air temperature. Turboshaft engine

and some of them have been in service for well over half a century (for example, the Lycoming T55), although the engine of today is a far relative of the original engine.

Limitations come in the form of limit speeds, temperatures and other operational constraints. For example, the N_{gg} speed is given as the nominal (design) 100% rpm, but it has upper limits of the order of 102–104%. Actual speeds can exceed 60,000 rpm on some small engines. There is generally a temperature limit in some section of the engine (inter-turbine temperature) or temperature at the exit of the last turbine stage, and the exhaust gas temperature (EGT). Operational constraints include minimum and maximum outside air temperature and flat rating data.

Data that are regularly missing include the overall pressure ratio, the design fuel flow rates, and the intake mass flow—all critical data for engine performance analysis. A few data are collected in Table 3.1. In the database shown, overall pressure ratios, Π, are below 17, and are notably lower than pressure ratios of modern high by-pass ratio engines. The main source of data for civilian helicopters is the Type Certificate, but for other engines one needs to carry out research across different databases.

From Table 3.1, we can infer some typical power/weight ratio (*specific power*): these range from just less than 2 kW/kg to over 10 kW/kg, growing rapidly with the engine power ratings. The trend is slightly biased toward newer engines. For example, the T53-L-701, one of the earlier versions of a family of turboshaft, appears slightly under-powered in comparisons with newer versions of the same family of engines, some of which have been converted into turboprops, Fig. 3.8.

3.3.1 Specific Fuel Consumption

There is no easy way to compare different turboshaft engines. One parameter that is often provided is the *specific fuel consumption*. This is defined as the ratio between the fuel flow and the net shaft power: $\text{SFC} = W_{f6}/P_{shaft}$. Contrary to common belief,

Table 3.1 Turboshaft engines data, static conditions, standard day, sea level; some data unavailable

Engine		W [kg]	TOP [kW]	MCP [kW]	MEP2 [kW]	Π	W_1 [kg/s]	Data
Turbomeca	Arriel 2C2	131	609	597	656	8.0	2.14	EASA E.001
Turbomeca	Arrius 2B2	112	479	432	554	8.4		
Turbomeca	RTM322-01/1	255	1518	1566	1669	14.2	4.52	EASA E.009
Rolls-Royce	C250 C20B/J	72	313	313	313	7.1	1.56	EASA E.052
Rolls-Royce	CTS-800-N	185	1014	955	1108	14.6	4.54	EASA E.232
General electric	T58-GE-8	139	912			8.3	5.61	
General electric	CT7-8	246	1879	1523	1879		> 20	EASA E.010
General electric	T64-GE-419	342	3570			14.9		
General electric	T700-GE-700	198	1210			17.0	4.5	
Rolls-Royce	T406(AE1107)	440	4586			16.7	16.0	Ref. [4]
Lycoming	T55-L-714A	377	3780	3620	3780	9.3		
Allison	T53-L-701	312	1082			7.4	4.85	
PZL	PZL-10W	143	662	574	846	7.0	4.50	EASA E.128

Weights sometimes quoted with/without reduction gear-box; data and/or type certificate sources in the right column. Where no data source is given, data are inferred from open source documents
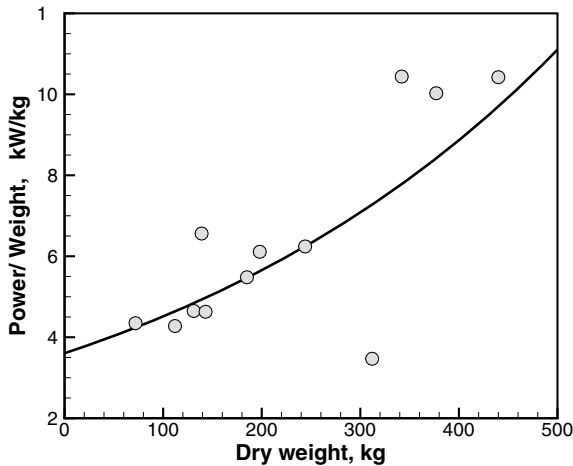

Fig. 3.8 Specific power data, P/W, for selected engines; power used is maximum continous power
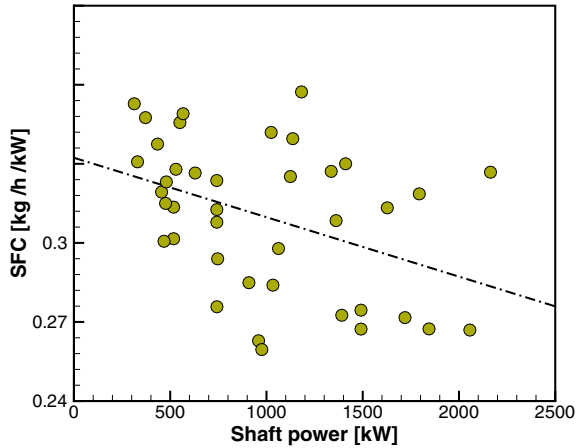
Fig. 3.9 Design SFC values for selected turboshaft engines (anonymised)

the SFC is *not a constant*. Its value depends on a large number of parameters and circumstances, and hence direct comparisons are impossible.

The physical units of the SFC are [mass/time]/[power]. In *International Units* (SI), SFC would be [kg/s/W], which is a rather small number. It is often converted to [kg/h/kW]. In the US, *Imperial Units* [lb/h/shp] are used, although these units are often neglected altogether in technical documentation and marketing brochures, and one needs to guess what the numbers mean.

A summary of SFC data available in the open domain is shown in Fig. 3.9. There is no evident correlation in performance, aside from a small improvements at high design power ratings. Is this sufficient to make an engine selection?

Aero engine performance depends on the jet fuel . Aviation fuel types are strictly regulated, and we refer to the relevant standard for their characteristics. For example, the commercial fuel Jet A1 has densities at 15 °Cin the range 0.775–0.840 kg/l, as reported by British Standards.[3] Military jet fuels include JP-4 and JP-5[4] At standard air temperature, the JP-4 has density of 0.751–0.802 kg/l, and JP-5 has a density of 0.788–0.845 kg/l.

Another important factor is the net caloric value, or the maximum chemical energy that can be converted to thermal energy. When fuel is burned, some energy is lost to heat in the water vapour, which is one of the products of combustion. In open systems such as turboshaft engines, this cannot be recovered. For this reason we use the "Lower Caloric Value" (LCV) of the fuel when establishing the required fuel flow rate, as opposed to the Higher Caloric Value (HCV) which assumes water is fully condensed. The LCV for Kerosene is 43 MJ/kg; the amount available for raising the temperature of the gas depends on the thermal efficiency of the engine,

[3] UK Ministry of Defence: Turbine Fuel, Kerosine Type, Jet A-1. DEF STAN 91-91, Issue 7, Amendment 3 (2015).

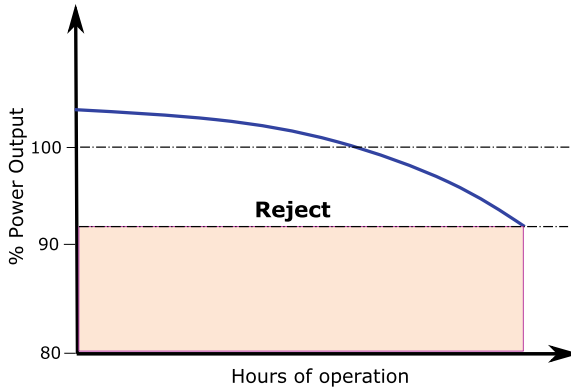[4] Turbine Fuel JP-4 and JP-5: Standard MIL-DTL-5624U (1998).

Fig. 3.10 Turboshaft power output deterioration

which is the ratio of useful work to the heat input during combustion. Typical values for turboshaft engines at design point are 0.25–0.35%, but depend on the operating altitude.

3.3.2   Engine Performance Degradation

When the engine is designed for a particular application, it is not unlikely that it is delivered with a slighter higher uninstalled shaft power. If we use normalised data, the engine manufacturer may be able to deliver an engine specification equivalent to 102% of the contracted power, interpreted for a *new engine, uninstalled, sea level, standard day*. Over time, the output power decreases for a number of factors, all related to deterioration effects in critical parts of the engine, due to thermal and mechanical fatigue, ingestion of particulate, mechanical erosion by lubricants or between metallic parts, etc. A power output curve may look like the one shown in Fig. 3.10. Depending on the customer, at 92–96% of the design output power would require an engine overhaul and maintenance, indicated as a "reject". In particulate-rich environments, the curve would feature a more rapid decrease in power output. When the rejection output is level, a compressor wash is triggered and some power out put is recovered, leading to a sawtooth shape in Fig. 3.10.

Engine rejection rates are often found to be much higher than predicted when operating in harsh environments such as desert conditions, littoral locations, and at sea. Mineral dust kicked up by rotor downwash or sea spray, contains silicates, carbonates, and sulphates, all of which attack substrates in different ways. Quartz is a very common mineral, and is particularly responsible for erosion of first stage compressor blades. However, this problem has been largely dealt with via the implementation of intake protection systems (see Sect. 3.5) and through application of

ceramic-metallic matrix erosion-resistant coatings, albeit at a cost. But deposition of finer-grained material continues to pose several problems.

Fouling of compressor blades arises when sub-micron and micron-sized particles get trapped the thicker, slow-moving boundary layers towards the trailing edge of the pressure surface, and adhere under van der Waals force. Larger particles avoid this fate either due to stored elastic energy being greater than the attractive forces, or due to the centrifuging action of the rotating airflow leading to their complete avoidance of the blades. Fouling is a common problem for turbo-machinery, leading to a loss of aerodynamic efficiency and subsequent reduction in pressure ratio across a compressor stage for a given input of work. This can often be recovered through washing during regular maintenance visits.

In the hot section of the engine, where combustor walls and turbine vanes and blades are located, deposition causes more permanent damage. This happens in several ways. Firstly, deposited mineral dust can form an in-situ melt that permeates the interstices of thermal barrier coatings and attacks the underlying metal, leading to embrittlement and increased risk of crack formation. Secondly, molten material that has accumulated may solidify if the engine is run at a lower power setting (cooler core temperature). This can then lead to a spalling mechanism arising from the mismatch in thermal expansion coefficient between the two materials.

In each case, the deposit formation, and the associated performance deterioration, has been shown to exhibit an asymptotic exponential growth with mass delivered (see Ref. [5]). The time constant of this growth is dependent on the type of dust encountered, and the engine operating conditions (gas temperature, relative velocity), and reflects the trade-off between deposition and shedding. By fitting an asymptotic shape to the total pressure loss across a stage, we are able to obtain the time constant of deterioration, τ, and the asymptotic total pressure loss ω_∞, represented here as a coefficient:

$$\Delta\omega = \Delta\omega_\infty \left(1 - e^{-\frac{C_{1,c}}{N_b \tau}}\right) \tag{3.2}$$

where ω is the total pressure loss coefficient, $C_{1,c}$ is the dust concentration, and N_b is the number of blades or vanes per stage. This can be used to predict the rate of performance deterioration associated with particulate fouling and deposition.

3.4   Engine Performance Envelopes

Turboshaft engines are adversely affected by atmospheric conditions in a way that other gas turbine engines are not. The key effects are flight altitude (or pressure altitude) and air temperature.

A first-principle analysis is done by correcting fuel flow and shaft power for the effects of altitude, which materialise in density, pressure and temperature decreasing with the altitude (in standard atmosphere). This relationship is:

$$\frac{W_{f6}}{\delta\sqrt{\theta}} = A_e + B_e \frac{P}{\delta\sqrt{\theta}} \tag{3.3}$$

where the coefficients A_e and B_e depend on the engine, P is the total shaft power. If there are n engines, then Eq. 3.3 will have the term P/n. At zero net shaft power, the fuel flow is $W_{f6} = A_e$. If both coefficients are constant, then there is a linear relationship at all altitudes between fuel flow and shaft power.

3.4.1 Engine Simulation Models

Engine simulation offers a wider possibility for exploring the engine envelope than any flight testing. It is faster, far less expensive and risky. The main drawback is the lack of reference data and validation procedures. With these caveats in mind, in recent years there has been a considerable amount of development in the area of aero-thermodynamic simulation of gas turbine engines. A number of sophisticated computer codes are available, such as the NASA Propulsion System [6, 7] (NPSS), the Gas Turbine Program GSP [8, 9], TurboMatch [10] and a number of other commercially available computer codes (for example, *GasTurb*).

One common feature of these computer codes is that they model the one-dimensional (gradients only along the gas path) gas flow across all the engine sections, both steady and unsteady, and are able to provide a sufficiently detailed map of the engine performance. A comparison between computer models has seemingly not been made available in current publications, but it is likely that some differences exist, not necessarily due to the core models, but also due to the use and integration of the input data. A model of the engine is shown in Fig. 3.11. The key systems of the engines are numbered from 1 (inlet) to 9 (exhaust).

Key temperatures are given at the exit of each system, $T_1 \ldots, T_5$, with TIT the inter-turbine temperature. The TIT is sometimes called $T_{4.5}$ (the exit of the high-pressure turbine) or $T_{4.6}$ (entry to low-pressure turbine).

The TIT or the total temperature at the exit of the last turbine stage T_5 are given as operational limits in the engine's *Type Certificate*. The temperature $T_4 > 1800\,\text{K}$ and the exhaust gas temperature (EGT) can be in well in excess of $500\,\text{K}$. The exhaust turbine temperature has limits between 550 and $750\,\text{K}$, from idle to take-off power, respectively.

One example of comparisons between different simulations is shown in Fig. 3.12. The lapse rate of the engine power is closer to $\sigma^{0.8}$ for the case of the GSP simulation and σ for the NPSS simulation (σ is the relative air density on a standard day). However, there are glaring differences between the two simulated data sets. The relationship $P(z) = P_{sl}\sigma^{0.8}$ is often used in first-order altitude analysis of rotorcraft.

Figure 3.13 shows a comparison between two different models of the T700 turboshaft engine and some reference data [11]. In this case we show the net torque at the engine shaft as a function of the fuel flow. The Q-W_{f6} only shows a constant bias (except the first point) on the reference data.
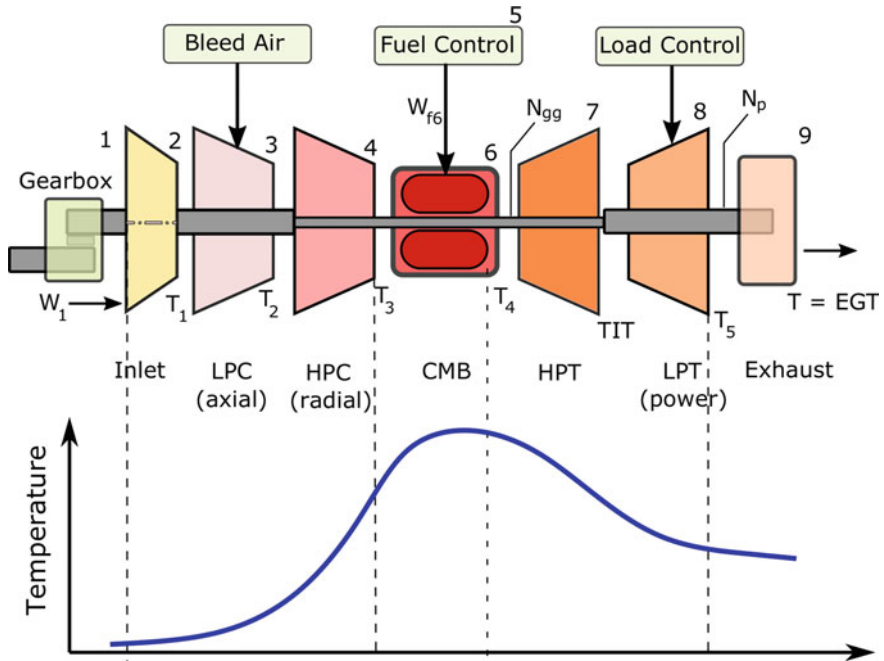
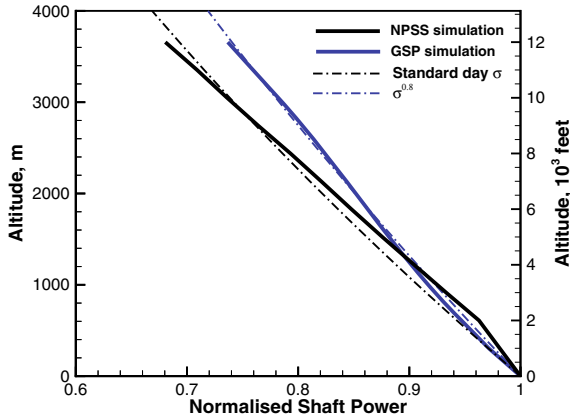**Fig. 3.11** One dimensional aero-thermodynamic model of a turboshaft engine

Fig. 3.12 Altitude-dependent shaft power of a model T700 turboshaft engine, simulated with GSP and NPSS
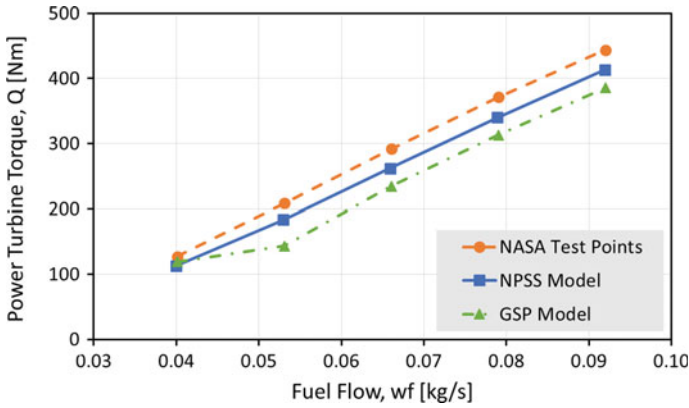
Fig. 3.13 Comparison between GSP and NPSS simulations of the T700 engines and reference data from NASA [11]. Courtesy of Matthew Ellis (University of Manchester)
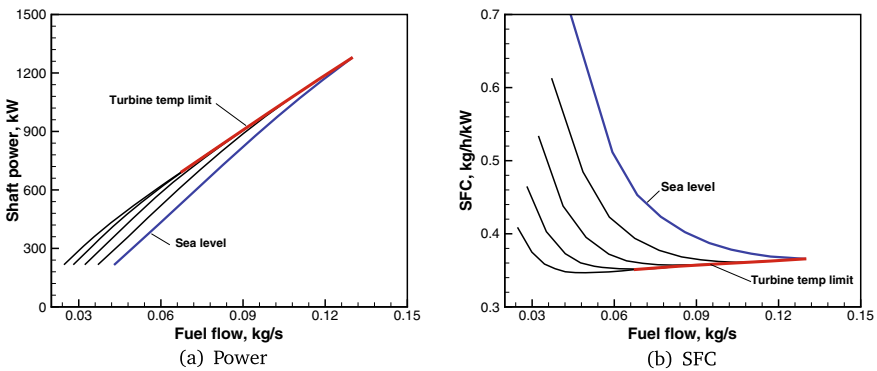

Fig. 3.14 Simulation of the T700 turboshaft engine on a standard day. Power and SFC lines at 2000 m/6560 feet intervals

A full simulation of the T700 engine is shown in Fig. 3.14, which displays the unistalled shaft power and the SFC on a standard day. Note how the SFC increases rapidly at low fuel flow rates.

3.4.2 Engine Emissions

Turboshaft engines do not fall within the ICAO regulations of emissions, and hence there is no obligation for engine manufacturers to report emissions characteristics as it is done for large turbofan engines. However, the exhaust emissions are equally important. Lacking rational reference data, we can only refer back to the sparse studies available in the technical literature, one of which, Ref. [12] clearly highlights
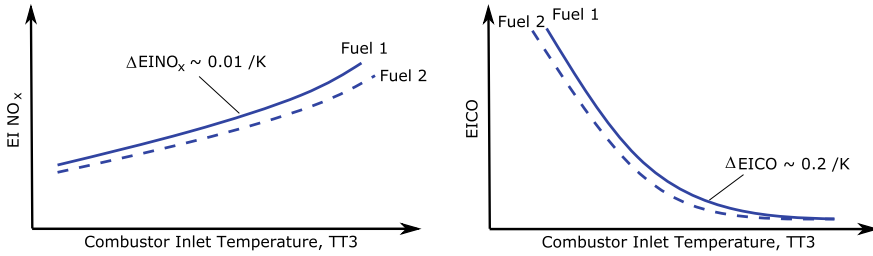
Fig. 3.15 Notional behaviour of some exhaust emission indices for a turboshaft engine

the difficulties of assessing the emissions for this type of vehicles, but it also proposes ways of providing estimates.

Emissions data that are of interest are CO (carbon-monoxide), NO_x (nitrogen oxides), UHC (uncombusted hydrocarbons), SO_x (sulphur oxides), non volatile particulate matter (mostly black carbon) and volatile organic compounds (VOC). Emissions of CO_2 are referred back to the fuel burn, since there is a constant multiplier between the fuel burn and the carbon emissions. This multiplier depends on the fuel and fuel-air ratio, but it is generally assumed to be 3.156 kg/kg of fuel.

Emissions other than CO_2 depend on fuel burn in non linear relationships. In fact, other factors intervene, in particular the entry conditions in the combustor, the maximum temperature and pressure in the combustor and the geometry of the combustor itself. At least one study of the emissions of the T700 turboshaft engine is available [13] and one on the T63 turboshaft [14]. A general trend of emission indices for NO_x and CO is displayed in Fig. 3.15. The data shown are emission indices, normally given as [g/kg] of fuel burned. Difference between aviation fuels have also been reported.

NO_x emissions increase with combustor temperature. Increasing combustor temperature in modern engines, due to higher compression ratios has caused this side effect. The opposite has taken place on the carbon-monoxide emissions, which is the product of incomplete combustion.

Emission assessments for helicopters is a far less formalised process than the ICAO-regulated turbofan engines. In part, this is due to the complexity of airborne operations carried out by this type of vehicles; in part we have a notable absence in emissions standards for this type of engines.

In order to begin making an assessment, we need to have average fuel flow rates and *time-in-mode* t_i estimates. A time-in-mode is the amount of time the engine runs at a given rpm, for example during idle, take-off, climb-out and cruise. The fuel burn for each mode i is $W_{fi} = W_{f6_i} t_i$:

$$W_f = \sum_i W_{f6_i} t_i \qquad (3.4)$$

Table 3.2 Times-in-mode for single and twin-engine turboshaft engines

	t_{ID} [min]	t_{AP} [min]	t_{TO} [min]	P_{ID} %	P_{AP} %	P_{TO} %
Single	5	3.5	3	7	38	78
Twin	5	5.5	3	6	32	66

ID ground idle; *AP* approach (descent and landing); *TO* take-off (hover and climb)

Values suggested for times-in-mode are indicated in Table 3.2, adapted from Ref. [12]. For each of the operating modes (ground idle, approach, take-off), we need an estimate of the fuel flow (which depends on the shaft power), and finally an estimate of emission indices for each chemical emission species.

We assume that the fuel flow to power relationship can be established by numerical simulation with one of the gas turbine methods described in Sect. 3.4.1, otherwise some empirical estimates are available. Hence, there is a suggestion of empirical relationships derived from testing, as given below:

$$
\begin{aligned}
\text{EI}_{\text{NO}_x} &\simeq 0.2113\, P_s^{0.5677} & [\text{g/kg}] \\
\text{EI}_{UHC} &\simeq 3819\, P_s^{-1.0801} & [\text{g/kg}] \\
\text{EI}_{\text{CO}} &\simeq 5660\, P_s^{-1.1100} & [\text{g/kg}] \\
\text{EI}_{nvPM} &\simeq 0.1056 + 2.3664 \times 10^{-4}\, P_s - 4.8 \times 10^{-8}\, P_s^2 & [\text{g/kg}] \\
\text{PM} &\simeq \text{EI}_{nvPM} / \tfrac{\pi e^{2.88}}{6} \left(\overline{d}_p^3 \right) & [-]
\end{aligned}
\tag{3.5}
$$

where the power P_s must be expressed in shaft-horsepower SHP (with a conversion factor 1 kW = 0.7457 SHP) and $\overline{d}_p$ is the mean particle diameter [nm]. At this point, it is possible to make a very approximate estimate of the LTO emissions. For example, for the NO_x we have

$$
\text{LTO NO}_x = 60\, n\, EI_{\text{NO}_x} \left(t_{ID} W_{f6_{ID}} + t_{TO} W_{f6_{TO}} + t_{AP} W_{f6_{AP}} \right) \quad [\text{g}]
\tag{3.6}
$$

since the fuel flow is in [kg/s] and the times-in-mode are given in minutes. For each operational mode, calculate the required power P; from the power, calculate the fuel flow W_{f6}; the fuel burn is calculated from the time-in-mode, and the corresponding emission of a chemical species is calculated from multiplying the emission index, Eq. 3.5, by the fuel burn in that mode. This procedure is further described in Sect. 3.6 below.

The procedure is clearly approximate because the emission indices only appear to depend on the shaft power and not on the specific engine, jet fuel, deterioration effects, as indicated in Fig. 3.15. However, with these approximations, we have the general behaviour illustrated in Fig. 3.16, which shows the case of a notional 1200 kW turboshaft engine. When the helicopter is operating in idle mode on the ground ($P \simeq$ 90 kW), emissions of carbon monoxide and uncombusted hydrocarbons are more than four times higher than the corresponding emissions at other operational modes.
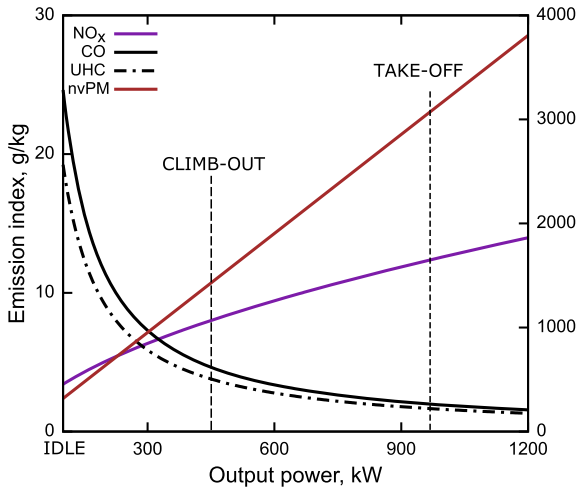
Fig. 3.16 Behaviour of some exhaust emission indices as a function of shaft power

This result is in agreement with complaints of poor air quality where helicopters operate near the ground. Some emission analysis methods have been published in the technical literature, Ref. [15] and some include the effects of the jet fuel composition [16].

A more detailed process for estimating emissions requires a mission analysis (Chap. 4). Mission optimisation can be carried out to minimise fuel burn and emissions. An alternative approach is to look at databases of flight trajectories for rotorcraft that use the standard ADS-B transponders, and simulate or 're-analyse' the trajectory using an accurate engine model.

3.5 Engine Intake Protection Systems

An intake protection system prevents particulate, dust and foreign object debris from being ingested into the engine, which can potentially have catastrophic consequences on the engine. This can be instantaneous damage or long deterioration or erosion of critical parts in the engine. An example of compressor blades erosion is shown in Fig. 3.17.

The amount of dust raised correlates directly to the average disk loading, and to a lesser degree the shape of the wake (number of trailing vortices—see Ref. [18]). For example, it was reported in Ref. [19] that dust concentrations at the rotor tips, at a height of 1.4 m, varied from 310 mg/m^3 for a Bell UH-1 to 2110 mg/m^3 for a Sikorsky MH-53. The corresponding disk loadings were 24 and 48 kg/m^2. Thus, a doubling of the disk loading caused a massively higher dust cloud concentration. Under these conditions, engine damage is inevitable without the use of intake protection. It must

Fig. 3.17 Example of compressor erosion, adapted from Ref. [17]. The image is reproduced under Crown Copyright, with permission from the Defence Science and Technology Laboratory (DSTL). DSTL is an executive agency of the UK Ministry of Defence (MoD)

be noted that concentration increases rapidly toward the ground (3200 mg/m^3 for the MH-53 at a ground height of 0.5 m). This is not the dust that will be ingested: concentration, particle size distribution depend on operational conditions and chemical composition depends on the ground conditions. In order to prevent such dust ingestion, helicopters operating on these harsh environments are equipped with intake particle separators. There are three types of systems, of which a full technology review is published in Ref. [20]:

1. Inertial Particle Separators (IPS): these separators can be an integral part of the intake or installed as add-ons in front of the engine. These systems are rather common, at least for military engines.
2. Vortex Tube Separators (VTS): these are packs of helix-shaped channels in front of the engine, which separate the air flow on the principle of inertia (as above), although particle collision dynamics plays an important part.
3. Inlet Barrier Filters (IBF): as the case of the vortex tubes, these are add-on separators that are installed at the inlet, and consist of fiber-based filtration principles.

For all separators, we have two very important performance parameters: the separation efficiency and the pressure loss at the inlet. Inevitably, there is a cross-correlation between these parameters and an engineering compromise is required. Separation efficiencies η_s are as follows: inertial particle separator $\eta_s \sim 80\%$; vortex tube separator: $\eta_s \sim 95\%$; inlet barrier filter $\eta_s \sim 99\%$. These data are based on a coarse test dust with particle diameters 2–200 μm, and a mean diameter $d_p = 38\,\mu$m.

The pressure loss at the inlet is either depending on the operating point (IPS, VTS), or growing with time (barrier filters). In the latter case, since there is a continuous accumulation of particulate within the filter layers, the free passage of the air flow into the inlet is obstructed, and this is the cause of increasing pressure losses. A

partial recovery of the pressure loss is achieved by cleaning and washing of the filter at specified intervals. A loss of inlet pressure requires the compressor to work harder in order to deliver the required pressure ratio in the combustor.

Pressure losses across a clogged filter can be as much as a few kPa if the rotorcraft engines rapidly ingest fine talc-like dust. In such circumstances, typically during a *brownout* or *dust landing* it may become necessary to operate a bypass system, in order to avoid stalling the compressor. The pressure loss, δP_{IPS}, follows a quadratic with engine mass flow rate, or dynamic pressure, q:

$$\delta P_{IPS} = c_1 q + c_2 q^2 \tag{3.7}$$

where c_1 and c_2 are empirical factors that depend on the geometry of the separator. In the case of inlet barrier filters, these are non-constant and depend on the degree of clogging.

In the diagram of Fig. 3.2, there in an indication of an IPS presence. In this case, the IPS is bolted in front of the engine, to the left in the drawing. With a high-speed IPS particles and gas are forced around a hump. The particulate would tend to follow the path of lower duct curvature and is thus separated by inertia. Larger particles, that enter the intake in a more ballistic fashion, may reach the scavenge by a favourable sequence of interactions with the duct walls, although the same mechanism has been known to lead to the inadvertent ingestion of sand and gravel.

These systems were first developed in the 1970s by GE for the T700 engine; more recently, they have been applied to the RTM322, Fig. 3.2, and other engines. Large flow speeds into engine (70–90 m/s) are possible, but to centrifuge particles particles with diameters $d_p < 25\,\mu$m requires that the flow accelerates rapidly, both linearly and angularly, which may result in large pressure losses, of the order ~ 1 kPa. Separation efficiency is good for particle diameters $d_p > 25\,\mu$m.

The particulate is scavenged radially by a pump, leaving a cleaner core gas into the engine. To cater for the increased mass flow rate, the intake area is enlarged. The use of the pump requires additional power, which is taken from the engine. The power loss can be as much as 10%. Clearly, this causes an overall loss in propulsive efficiency, since a small part of the work has to be done to provide clean air. For this reason, particle separators must only be used when operating in harsh environments; they are not a standard piece of equipment. *A life-cycle analysis is required for an overall cost-benefit assessment*. Additional costs that would be considered in such an analysis include: system weight, maintenance burden, drag, reliability, integration, physical envelope.

3.6 Airframe-Engine Integration

There are considerable issues in the integration of a power plant onto an helicopter aircraft. We only consider the operational cases, when computer simulation is required. This is illustrated in the flowchart of Fig. 3.18.
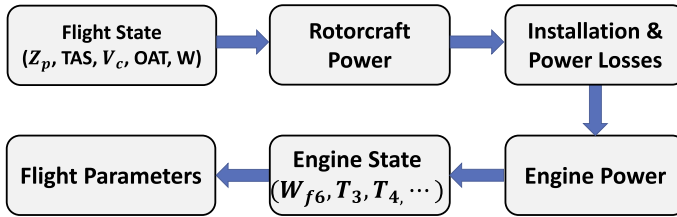
Fig. 3.18 Flowchart for calculating the engine-airframe integration

To begin with, we need to establish the flight conditions. These include at least the gross weight, flight speed, climb rate, flight altitude, atmospheric temperature, and possibly other parameters. This flight state is used to calculate the gross power required to fly at that condition, in trimmed state. The actual engine power depends on a number of integration factors, including transmission losses, intake and exhaust losses, presence of particle separators, and ageing effects (see also Fig. 3.10). Since there is often a need of compressor bleed air, that contributes to a relative reduction in air flow, or the reduction in net shaft power—this is an installation effect, which can be anything up to 20% of total power. Other effects include exhaust back pressure, due to friction or otherwise (of the order of 1%) and in case of military vehicles with infra-red suppression systems there is also a back pressure loss due to this additional system (in greater measure, presumably up to 15% of power).

At this point, there is a power/torque requirement, and the engine gas dynamics problem is solved in inverse mode. This means that we need to trim the fuel flow W_{f6} to deliver the required shaft power. Once a solution is achieved, that corresponds to an engine state that has several aero-thermodynamic parameters of interest: temperatures and pressures at critical sections of the engine, mass flow rates, etc. Finally, flight parameters are calculated, such as the specific air range and the specific endurance.

3.7   Case Study: Optimal Operation of a Multi-engine Helicopter

An interesting case for optimal cruise performance with one engine inoperative has been proposed in Ref. [21] for the three-engined AW101 *Merlin* helicopter. The following case study is based on the approach that it is possible to gain fuel efficiency at some flight conditions with one engine inoperative.

We discussed the features of twin-engine rotorcraft, but very little was reported on three-engine configurations. Now consider the latter case. We have a three-engined rotorcraft powered by RTM322 turboshafts. Flying at the loiter speed (approximate), is there any gain in disengaging one engine for the purpose of improving fuel flow characteristics?—What is the effect on the SFC?

(a) Mil-14   (b) Mil-17

Fig. 3.19 Examples of three-engined helicopters: Mil-14 in search-and-rescue configuration and Mil-17 military aircraft. Photos courtesy of Filip Modrzejewski (2019)
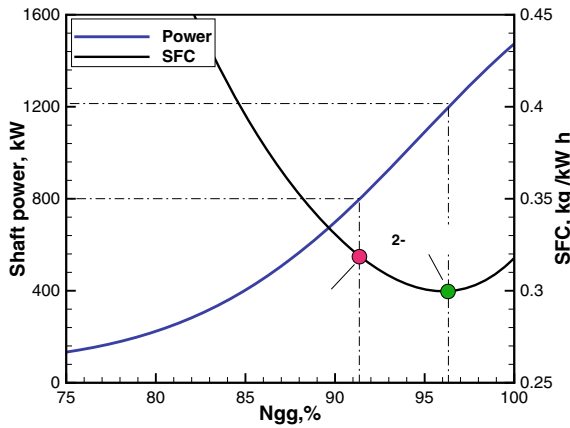

Fig. 3.20 Twin- versus three-engine turboshaft operation

Photographs of three-engined rotorcraft are shown in Fig. 3.19. In the case of the Mil-17, note the inertial particle separators on the two lower engines. The central higher engine is more protected from the ingestion of dust and particulate and is thus not equipped with this system.

For the purpose of this discussion, assume that at this flight condition (steady level flight) we require a total of 2400 kW, which delivered in equal measure by the three engines (800 kW/engine). The performance curve is shown in Fig. 3.20, which displays both power and SFC as a function of the gas turbine speed, N_{gg}. The data have been generated by one of the engine simulation programs mentioned earlier (GSP). We demonstrate that in this case there is some efficiency gain in operating the rotorcraft as a twin-engine—with some caveats.

To begin with, the three-engine operation would require $N_{gg} \simeq 91.5\%$ to meet the 800 kW output power demand, with an SFC $\simeq 0.32$ kg/h/kW. The twin-engine

operation would require a power output $1200\,kW$/engine. This is achieved with $N_{gg} \simeq 93\%$, although it has the benefit of *decreased* SFC to $\sim 0.30\,kg/h/kW$. This means a reduction in SFC by over 6%, which is considerable. A similar analysis could be carried out for twin-engine rotorcraft operating as a single engine [22], since there are fuel consumption benefits at higher engine loads.

Operating at higher rpm may cause an increase in direct operating costs, particularly on the maintenance side of the costs, and this is not evidenced in the graph, because the graph only shows the effects of fuel burn. Furthermore, the safety implications are not discussed, and these need to be carefully addressed, if there is a sudden need of a power supply. It is well known that the restart time of a gas turbine engine can be several seconds, and in emergency situation there can be loss of speed and altitude; this limits the safe envelope of the intended OEI flight. We conclude that a *complete analysis of engine performance needs to take into account factors that are beyond fuel burn.*

References

1. O'Brien DM, Calvert ME, Butler SL (2008) An examination of engine effects on helicopter aeromechanics. In: AHS specialist conference on aeromechanics, San Francisco, Jan 2008
2. Wilson HK (1991) Drive system for tiltrotor aircraft. US Patent 5,054,716, Oct 1991
3. Weden CJ, Coy JJ (1984) Summary of drive-train component technology in helicopters. Technical report TM 83726, NASA, Oct 1984
4. Arvin JR, Bowman ME (1990) T406 engine development program. In: ASME gas turbine & aeroengine congress, ASME 90-GT-245, Brussels, June 1990
5. Döring F, Staudacher S, Koch C (2017, June) Predicting the temporal progression of aircraft engine compressor performance deterioration due to particle deposition. In: Volume 2D: Turbomachinery. ASME, p V02DT48A007. https://doi.org/10.1115/GT2017-63544
6. Lytle JK (2000) The numerical propulsion system simulation: an overview. Technical report NASA TM-2000-209915, NASA, June 2000
7. Jones SM (2007) An introduction to thermodynamic performance of aircraft gas turbine engine cycles using the numerical propulsion system simulation code. Technical report NASA TM-2007-214690, NASA, Mar 2007
8. Visser WPJ, Broomhead MJ (2000) GSP: a generic object-oriented gas turbine simulation environment. In: ASME gas turbine conference, ASME 2000-GT-0002, Munich, Germany. Program available from www.gspteam.com
9. Visser WJP, Kogenhop O, Oostveen M (2004) A generic approach for gas turbine adaptive modeling. J Eng Gas Turbines Power 128(1):13–19. https://doi.org/10.1115/1.1995770
10. Pachidis V, Pilidis P, Marinai L, Templalexis I (2007) Towards a full two dimensional gas turbine performance simulator. Aeronaut J 111(1121):433–442. https://doi.org/10.1017/S0001924000004693
11. Duyar A, Zu G, Litt JS (1995) A simplified model of the T700 turboshaft engine. J Am Helicopter Soc 40(4):62–70
12. Rindlisbacher T, Classey L (2015) Guidance on the determination of helicopter emissions. Technical report, FOCA, Bern, Switzerland, Dec 2015
13. Cohen JD (1984) Analytical fuel property effects—small combustors. In: Grobman J (ed) Assessment of alternative aircraft fuels, NASA CP 2307, pp 89–98
14. Kinsey JS, Corporan E, Pavlovic J, DeWitt M, Klingshirn C, Logan R (2019) Comparison of measurement methods for the characterization of the black carbon emissions from a T63

turboshaft engine burning conventional and Fischer-Tropsch fuels. J Air Waste Manag Assoc 69(5):576–591. https://doi.org/10.1080/10962247.2018.1556188

15. Ortiz-Carretero J, Castillo Pardo A, Goulos I, Pachidis V (2018) Impact of adverse environmental conditions on rotorcraft operational performance and pollutant emissions. ASME J Eng Gas Turbines Power 140(2). https://doi.org/10.1115/1.4037751

16. Li-Jones X, Penko P, Williams S, Moses C (2007) Gaseous and particle emissions in the exhaust of a T700 helicopter engine. In: Volume 2: Turbo expo 2007 of turbo expo: power for land, sea, and air, 5 2007. https://doi.org/10.1115/GT2007-27522

17. Martin N (2019) Gas turbine engine environmental particulate foreign object damage. Technical report STO-TR-AVT-250, NATO. https://doi.org/10.14339/STO-TR-AVT-250

18. Milluzzo J, Gordon Leishman J (2010, July) Assessment of rotorcraft brownout severity in terms of rotor design parameters. J Am Helicopter Soc 55(3):32009–320099

19. Cowherd C (2007) Sandblaster 2 support of see-through technologies for particulate brownout—task 5. US Army Aviation & Missile Command, Technical report, Oct 2007

20. Bojdo N, Filippone A (2010) Turboshaft engine air particle separation. Prog Aerosp Sci 46:224–245

21. Massey C, Violante T, Highams L (2018) One engine inoperative cruise for mission performance optimisation. In: Proceedings of the 74th annual vertical flight society forum, Phoenix, AZ, May 2018

22. Kerler M, Erhard W (2014) Evaluation of helicopter flight missions with intended single engine operation. In: European rotorcraft forum, Sept 2014

Prof. Antonio Filippone is at the School of Engineering, University of Manchester, where he specialises in aircraft and rotorcraft performance, environmental emissions aircraft noise, and engine performance.

Dr. Nicholas Bojdo is at the School of Engineering, University of Manchester, where he specialises in aero engine propulsion, intake design, engine air particle separator systems, dust and volcanic ash ingestion, engine deterioration.